Spin Hall effect and spin filtering in ballistic nanojunctions

2007 J. Phys.: Condens. Matter 19 395019

(http://iopscience.iop.org/0953-8984/19/39/395019)

IOP PUBLISHING JOURNAL OF PHYSICS: CONDENSED MATTER

J. Phys.: Condens. Matter **19** (2007) 395019 (14pp) doi:10.1088/0953-8984/19/39/395019

Spin Hall effect and spin filtering in ballistic nanojunctions

S Bellucci[1], **F Corrente**[1,2] **and P Onorato**[1,3]

[1] INFN, Laboratori Nazionali di Frascati, PO Box 13, 00044 Frascati, Italy
[2] Dipartimento di metodi e modelli matematici per le scienze applicate, Universitá di Roma 'La Sapienza', via A Scarpa, 16, 00161 Roma, Italy
[3] Department of Physics, 'A Volta', University of Pavia, Via Bassi 6, I-27100 Pavia, Italy

Received 8 March 2007
Published 30 August 2007
Online at stacks.iop.org/JPhysCM/19/395019

Abstract

We discuss the behaviour of a four-probe ballistic cross nanojunction patterned in a two-dimensional electron gas (2DEG) by taking into account the spin–orbit (SO) coupling due to the in-plane electric field.

We propose a new scheme of spin filtering based on this SO interaction in the regime of the so-called quenching of the spin Hall effect by discussing the geometrical effects on the transport with a semiclassical approach. We show that a pure spin current is induced in the transverse probes when an unpolarized charge current is injected through their longitudinal leads. We relate the spin conductance in the transverse probes to the charge conductance through the longitudinal leads.

We also demonstrate that the flow of a longitudinal unpolarized current through the junction will induce a spin accumulation which has opposite signs for the two lateral probes.

(Some figures in this article are in colour only in the electronic version)

1. Introduction

In recent years the increasing interest in spin-based information processing, and the related phenomenon known as spin Hall effect, fomented the field of semiconductor spintronics [1, 2]. Several fundamental quantum phenomena which involve electron spin have been investigated in order to generate and measure pure spin currents, i.e., those not accompanied by any net charge current. Among these studies many are focused on the role of the spin–orbit (SO) coupling in condensed matter systems in order to obtain a pure spin Hall current.

The Hall effect is a typical phenomenon concerning electric conduction [3]. A current flowing in a thin conductor in the presence of a magnetic field experiences a Lorentz force depending on the electric charge. This produces the splitting of the current: negative charges and positive ones flow in mutually opposite directions. Thus the inhomogeneous charge

distribution generates a potential difference: the Hall effect refers to the potential difference (Hall voltage) on opposite sides of a thin sheet of conducting or semiconducting material in the form of a 'Hall bar' through which an electric current is flowing, created by a magnetic field applied perpendicularly to the Hall element.

A similar effect subsists for the spin current in a conductor, and it is called the spin Hall effect (SHE) [4]. There are two kinds of SHE: extrinsic [4] and intrinsic [5–7]; the former is due to the scattering with impurities in the lattice of the conductor, and the latter is due to the electric field that produces an effect on the spin currents similar to that of the Hall effect on charge currents.

The spin–orbit coupling (SOC) plays a central role for understanding the SHE. The devices which we consider are low-dimensional electron systems created by quasi-one-dimensional (Q1D) devices patterned in a two-dimensional electron gas (2DEG). The confinement of the electrons is obtained by external potentials which generate different SOC [8], such as the Rashba SOC (the α-SOC term due to the quantum-well potential [9] that confines electrons to a 2D layer) and the confining SOC (the β-SOC term arising from the in-plane electric potential that is applied in order to squeeze the 2DEG into a Q1D channel [9, 10]).

In α-SOC we have an electric field orthogonal to the motion plane. A useful way to describe the effect of this field is to use an effective magnetic field coplanar to the motion plane and orthogonal to the electrons velocity. The form of α-SOC in the Hamiltonian is [8, 11, 12]

$$\hat{H}_{\mathrm{SO}}^{\alpha} = \frac{e\lambda^2}{\hbar}\left(\sigma_x p_y - \sigma_y p_x\right). \tag{1}$$

The typical expression of the β-SOC, generated by an electric field applied in the same plane of a current flowing through the 2DEG, is given by [13–17]

$$\hat{H}_{\mathrm{SO}}^{\beta} = \frac{\lambda^2}{\hbar}\hat{\sigma}_z\left[\nabla V(x) \wedge \hat{p}\right]. \tag{2}$$

A useful way to describe the effect of the confining SOC is to represent it in terms of an effective magnetic field perpendicular to the motion plane.

Here we discuss the presence of the SHE in nanojunctions formed by crossing Q1D devices in the ballistic regime. This regime is realized when the flow of electrons in a device is not perturbed by impurities of the lattice, or when the dimension of the device is very large compared to the electrons' mean free path. When these conditions are satisfied, one of the consequences is that we can relate the conductance to the quantum mechanical transmission coefficients, $T_{n,m}$. One of the fundamental tools of this argument is the Büttiker–Landauer formula [18]. This formula yields the conductance of a system at $T = 0$ K in terms of the $T_{n,m}$,

$$G = 2\frac{e^2}{h}\sum_{m,n} T_{m,n}. \tag{3}$$

For a multiprobe device the Landauer formula was extended by Büttiker, starting from the formula

$$I_p = \sum_q \left(G_{qp}V_p - G_{qp}V_q\right) = \sum_q G_{pq}\left(V_p - V_q\right), \tag{4}$$

which relates charge currents in every single probe to the potential in all other probes by the conductance G_{pq}. Treating the spin currents in the same way, it is possible to obtain the following relation for the spin currents [19]:

$$I_p^s = \frac{\hbar}{2e}\sum_q \left(G_{pq}^s V_p - G_{qp}^s V_q\right). \tag{5}$$

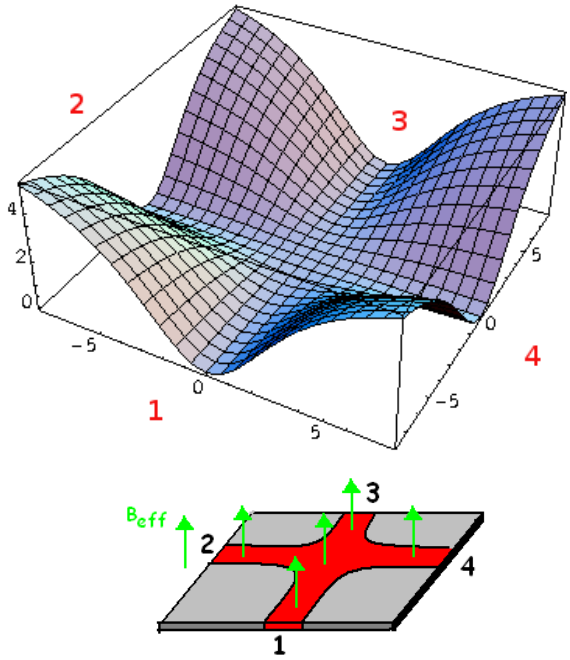

Figure 1. The mesoscopic junction (top), and 3D plots of the potential $V_c(x, y)$ which describes the nanojunction (bottom). The numbers indicate the index of the leads.

The presence of the SHE can be argued by the presence of a spin current or a spin accumulation. In [20], the authors demonstrated that the flow of a longitudinal unpolarized current through a ballistic 2DEG with α-SOC will induce a nonequilibrium spin accumulation which has opposite signs for the two lateral edges. The discussion was extended with the investigation of the SHE in multiprobe ballistic SO-coupled semiconductor bridges, [19] i.e., a device in which longitudinal leads are attached to a ballistic quantum-coherent 2DEG in semiconductor heterostructures [19, 20]. The latter devices can be assumed as a crossing junction between two Q1D wires[4], such as the one shown in figure 1. Thus the flow of a longitudinal ($1 \rightarrow 3$) unpolarized current through a ballistic X junction with α-SOC will induce a spin accumulation which has opposite signs for the two lateral probes (2 and 4) and could be the main observable signature of the SHE in this device [19, 20]. However, in Q1D devices the effects of the β-SOC can also be relevant [14–17] by giving a localization of the spin currents in a Q1D wire [13]. It follows that the value of the spin accumulation predicted for the β-SOC in nanometric cross junctions could be of the same order of magnitude, or larger, than the one predicted in [20] and due to a quite strong α-SOC.

The small strength of the effective magnetic field due to the β-SOC and the junction shape suggest that the device works in a regime analogous to the one known as the *quenching of the Hall effect* [15]. This regime corresponds to the one where, in the presence of a quite small external magnetic field, B, a suppression of the Hall resistance or a negative Hall resistance, R_{H}, was measured, as shown in [21]. The quenching of the Hall effect presumably depends on the geometry of the junction, which plays its role when the magnetic field is small. Instead, if there is a strong magnetic field, the geometry of the junction is less important. This aspect is

[4] The width W of each Q1D corresponding to the device proposed in [20] ranges from ∼25 nm to 100 nm.

very simple to understand: the geometry of the junction is represented in the Hamiltonian as an electric potential; when the magnetic field is smaller than the junction potential the former is more important in the description of our model. Instead, the opposite happens when we deal with strong magnetic fields.

In this paper we discuss the spin polarization of the current in the presence of β-SOC in X-shaped [15] four-probe (figure 1) nanometric cross junctions. We focus on single-channel transport and investigate with a numerical semiclassical approach the spin accumulation in the transverse leads and the correlated spin and charge conductance.

Section 2 is devoted to the description of the junction, to the corresponding confining potential and to a short introduction to the quenching of the Hall effect in cross junctions. In section 3 we introduce the theoretical model, we calculate the spin and charge conductance based on the Büttiker–Landauer formalism and we present our method to perform the computation of the conductances by a semiclassical construction. In section 4 we discuss our results by focusing on the spin Hall currents which flow through a four-probe cross junction and then we proceed to the analysis of spin accumulation along the leads. In section 5 we present our conclusions by also giving some details about the feasibility of the discussed device.

2. Q1D cross junctions and quenching of the Hall effect

Quantum wires (QWs or nanowires) are the fundamental element in the construction of the devices that we analyse here. A QW is usually defined as an electrically conducting wire having a width, W, smaller than 1000 Å [22] and a length, L, up to some microns (here we think of a QW where $W \sim 5$–100 nm) in which quantum effects affect the transport properties. As such, they are often referred to as 1D materials. Nanowires have many interesting properties that are not seen in bulk or 3D materials. This is because electrons in nanowires are quantum confined laterally and thus occupy energy levels that are different from the traditional continuum of energy levels or bands found in bulk materials. Peculiar features of this quantum confinement exhibited by certain QWs manifest themselves in discrete values of the electrical conductance. Such discrete values arise from a quantum mechanical restraint on the number of electrons that can travel through the wire at the nanometre scale. These discrete values are often referred to as the quantum of conductance, and they are given by integer values of $\frac{2e^2}{h}$. The conductivity of a nanowire is expected to be much smaller than that of the corresponding bulk material.

In line with [23], from a theoretical point of view, the lateral confining potential of a QW is usually defined by a parabolic confining potential along the transverse direction, $\hat{x}$, with strength ω_d:

$$V_c(x) = \frac{m}{2}\omega_d^2 x^2.$$

It will be useful for further development to introduce the length

$$l_\omega^2 = \frac{\hbar}{m\omega_d} \tag{6}$$

corresponding to the effective width of the QW.

A four-probe cross junction is formed by two perpendicularly crossing QWs (see figure 1). In this device the electric potential that confines electrons inside the wires is not exactly known.

In our model the confining action is wielded by a confining potential $V(\mathbf{x})$. The simplest way is to use a potential that will be parabolic along the shape we want for the junction in figure 1 (top). Adding to this the information that the potential plausibly has a minimum in the centre of the junction we can realize that a good model for the potential (see figure 1 (bottom)) is

$$V_X(\mathbf{x}) = \frac{m\omega_d^2 R^2}{2}\frac{x^2y^2}{(R^2+x^2)(R^2+y^2)}, \tag{7}$$

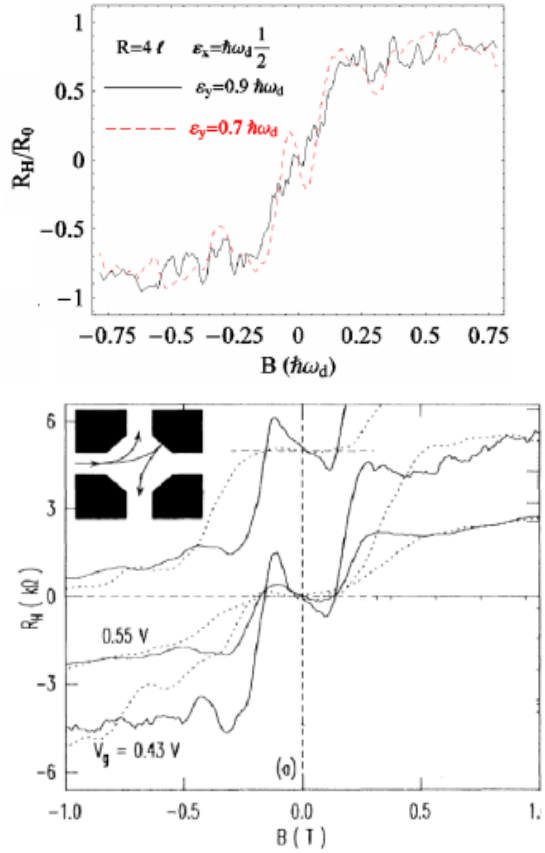

Figure 2. Top: calculated $R_{\rm H}$ versus B for two different values of the Fermi energy (experimentally corresponding to the gate voltage, $V_{\rm g}$). Here B corresponds to $\hbar\omega_c = \hbar eB/(m^*c)$ in units of $\hbar\omega_d$. At small B it is clear that a quenched region is present, where the Hall resistance, $R_{\rm H}$, is negative. Bottom: measured $R_{\rm H}$ versus B for the device in [21]; the crossing wires have a real width $W_R \sim 200$ nm and an effective one $W \lesssim 60$ nm. It follows that $\hbar\omega_d \sim 6$ meV, while the range of B ($\pm 0.75\hbar\omega_d$) corresponds to a B value which ranges between -1 and 1 T (see [12]). This allows for a comparison with the results shown in figure 1 of [21].

where l_ω can be related to the width, W, of the QWs, while R is related with the radius of the crossing zone.

As we mentioned above, the strength of the effective magnetic field due to the SOC is quite small. Thus we want to analyse a device, such as the nanojunction, where relevant effects on the transport properties also appear at small values of a real or effective magnetic field.

The transport through micrometric ballistic junctions (i.e., a cross junction between two narrow QWs in a 2DEG, also known as a four-probe junction) was largely investigated about 20 years ago. Several magneto-transport anomalies were found in these devices, among these the quenched or negative Hall resistance, bend resistances and a feature known as the last Hall plateau.

The quenching of the Hall effect is an attenuation of the Hall resistance which is observable when a low-intensity (typical values for the quenching in the device of [21] are $B \lesssim 0.2$ T) magnetic field is present. This attenuation is accentuated near the origin, as shown in figure 2 (bottom). One of the goals of our computational model is to take into account the quenching

within a good approximation. If we consider an idealized junction with sharp edges, the Hall effect manifests itself in a monotonic way, also when there is a low-intensity magnetic field. However, in order to describe the device we are studying correctly, we need to predict the so-called quenching of the Hall effect. This phenomenon is essentially due to the rounded corners present in every (real) device. The rounded edges contribute to the overall field, and manifest their presence by a negative electrical resistance.

The results of our simulations can be compared with the experimental data reported in [21] and turn out to support the validity of our approach.

3. Theoretical model and computational approach

3.1. Model and effective magnetic field

The overall Hamiltonian reads

$$H = \frac{\mathbf{p}^2}{2m} + V(\mathbf{x}) + H_{\mathrm{SO}}^{\beta} \tag{8}$$

where

$$H_{\mathrm{SO}}^{\beta} = \frac{\lambda^2}{\hbar}\sigma_z \left[\nabla V(\mathbf{x}) \wedge \left(\mathbf{p} + \frac{e}{c}\mathbf{A}\right)\right]_z \tag{9}$$

is the term of the Hamiltonian for β-SOC with $\lambda = \frac{\hbar}{(2mc)}$. In our case we have just the third component of the coupling because the motion orthogonal to the plane of the 2DEG is quantum mechanically frozen and we assume that there are no external magnetic fields, so $\mathbf{A} = 0$. It is important to observe that the third spin component is conserved, since the Hamiltonian commutes with it.

The Hamiltonian of an electron of a 2DEG moving in our device is then

$$H = \frac{\mathbf{p}^2}{2m} + \frac{\lambda^2}{\hbar} e\,(\mathbf{E}(\mathbf{x}) \wedge \mathbf{p})_z\,\sigma_z + V(\mathbf{x}) = \frac{\pi^2}{2m} + V(\mathbf{x}) - me^2\frac{\lambda^4}{2\hbar^2}\,|\mathbf{E}(\mathbf{x})|^2\,,$$

where $\pi_i = (p_i - \epsilon_{ijz}\frac{\lambda^2}{\hbar} m^* e E_j \sigma_z)$ and $\mathbf{E}(\mathbf{x}) = \nabla V(\mathbf{x})$. The commutation relation

$$\left[\pi_x, \pi_y\right] = -\mathrm{i}\hbar\frac{e}{c} B_{\mathrm{eff}}(\mathbf{x})\sigma_z \tag{10}$$

is the same as for a charged particle in a magnetic field, except that the sign of B_{eff} depends on the spin direction along z.

In the special case of a QW, $e\nabla V_{\mathrm{c}}(\mathbf{r}) \equiv m\omega_d^2(x, y, 0)$. Hence the effective magnetic field reads

$$B_{\mathrm{eff}} = \frac{\lambda^2}{\hbar}\,\frac{m^2\omega_d^2 c}{e} \equiv \frac{\beta}{\hbar l_\omega}\frac{mc}{e}, \tag{11}$$

where $\beta \equiv \lambda^2 m^* \omega_d^2 l_\omega$. Thus B_{eff} is orthogonal to the 2DEG directed upward or downward, according to the spin polarization along the z direction.

Introducing the effective cyclotron frequency $\omega_c = \frac{\beta}{\hbar l_\omega}$ ($\omega_c/\omega_d = \lambda^2/l_\omega^2$), the constant $\tilde{\omega}_d^2 = \omega_d^2 - \omega_c^2$ and the total frequency $\omega_T = \sqrt{\tilde{\omega}_d^2 + \omega_c^2}$, equation (8) reads

$$H = \frac{\tilde{\omega}_d^2}{\omega_T^2}\frac{p_y^2}{2m_e} + \frac{p_x^2}{2m_e} + \frac{m\omega_T^2}{2}(x - X_0)^2, \tag{12}$$

where $X_0 = s\frac{\omega_c p_y}{\omega_T^2 m_e}$ and $s = \pm 1$ corresponds to the spin polarization along the z direction. Notice the analogy with the Hamiltonian corresponding to one electron in the QW when an external transverse magnetic field is present.

3.2. Spin Hall conductance and Büttiker formalism

The mesoscopic experiments on quantum Hall cross junctions challenge of the theoretical interpretation of multiterminal transport measurements. As we discussed above, Büttiker [18] provided an elegant solution to this problem in the form of a multiprobe formula [18] in equation (5), which relates, via the conductance coefficients G_{pq}, the charge current $I_p = I_p^{\uparrow} + I_p^{\downarrow}$ in probe p to the voltages V_q in all other probes attached to the sample.

In order to study the spin-resolved charge currents I_p^{σ} ($\sigma = \uparrow, \downarrow$) we replace $I_p \to I_p^{\sigma}$ and $G_{pq} \to G_{pq}^{\sigma\sigma'}$. This viewpoint allows us to extract the multiprobe formulae for the spin-resolved charge currents [24, 25] I_p^{σ}, while the spin current flowing through probe p can be defined as

$$I_p^s = \frac{\hbar}{2e}(I_p^{\uparrow} - I_p^{\downarrow}) = \frac{\hbar}{2e}\sum_q [G_{qp}^{\text{out}} V_p - G_{pq}^{\text{in}} V_q], \tag{13}$$

where $G_{pq}^{\text{in}} = G_{pq}^{\uparrow\uparrow} + G_{pq}^{\uparrow\downarrow} - G_{pq}^{\downarrow\uparrow} - G_{pq}^{\downarrow\downarrow}$ and $G_{pq}^{\text{out}} = G_{pq}^{\uparrow\uparrow} + G_{pq}^{\downarrow\uparrow} - G_{pq}^{\uparrow\downarrow} - G_{pq}^{\downarrow\downarrow}$. Taking into account the spin conservation of our Hamiltonian we note that $G_{pq}^{\uparrow\downarrow} = G_{pq}^{\downarrow\uparrow} = 0$. At zero temperature, the spin-resolved conductance coefficients read $G_{pq}^{\sigma\sigma'} = \frac{e^2}{h}\sum_{ij} |\mathbf{t}_{ij,\sigma\sigma'}^{pq}|^2 = \frac{e^2}{h} T_{pq}^{\sigma\sigma'}$, where summation (i, j) is over the conducting channels in the leads (in the following we limit ourselves to just one channel).Thus the G coefficients are obtained, according to the Landauer formula, as the probability for a spin-σ' electron incident in probe q to be transmitted to probe p as a spin-σ electron, $T_{pq}^{\sigma\sigma'}$.

In order to test our approach by a comparison with the experiments, we first analyse the regime corresponding to the quenching of the Hall effect and we neglect the spin effects. Thus, by applying the Büttiker formalism [18] in a four-fold symmetric junction, such as the one shown in figure 1, we are able to compute the Hall resistances, R_{H}, as a function of the T_{pq} [26]:

$$R_{\text{H}} = R_0 \frac{T_{21} - T_{41}}{T_{21}^2 + T_{41}^2 + 2T_{31}(T_{21} + T_{31} + T_{41})}, \tag{14}$$

with $R_0 \propto h/e^2$.

Now we want to discuss the spin-dependent case in the presence of β-SOC. The commutation relation $[H, \sigma_z]$ in this system implies

$$T_{pq}^{\uparrow\downarrow} = T_{pq}^{\downarrow\uparrow} = 0 \Rightarrow G_{pq}^{\uparrow\downarrow} = G_{pq}^{\downarrow\uparrow} = 0,$$

so that $G_{pq}^{\text{in}} = G_{pq}^{\uparrow\uparrow} - G_{pq}^{\downarrow\downarrow}$ and $G_{qp}^{\text{out}} = G_{qp}^{\uparrow\uparrow} - G_{qp}^{\downarrow\downarrow}$.

Since the total charge current I_p depends only on the voltage difference between the probes in figure 1, we set one of them to zero (e.g., $V_3 = 0$ is chosen as the reference potential) and apply the voltage V_1 to the system. Imposing the requirement $I_2 = I_4 = 0$ for the voltage probes 2 and 4 we can specify the $V_2/V_1 = V_4/V_1 \equiv 1/2$ [19]. Thus, following [19], we can obtain the spin Hall conductance as

$$\begin{aligned} G_{\text{sH}} &= \frac{\hbar}{2e}\frac{I_2^{\uparrow} - I_2^{\downarrow}}{V_1 - V_3} \\ &= \frac{\hbar}{2e}\left[(G_{12}^{\text{out}} + G_{32}^{\text{out}} + G_{42}^{\text{out}})\frac{V_2}{V_1} - G_{42}^{\text{in}}\frac{V_4}{V_1} - G_{21}^{\text{in}}\right]. \end{aligned} \tag{15}$$

This quantity is measured in units of the spin conductance quantum $e/4\pi$. Analogously we are able to compute the corresponding longitudinal charge conductance

$$G_L = \frac{e^2}{h}\frac{I_3}{V_1} = \frac{\hbar}{2e}\left[G_{31} + G_{32}\frac{V_2}{V_1} + G_{34}\frac{V_4}{V_1}\right]. \tag{16}$$

The symmetry of the device is reflected by the transmission coefficients, so that $T_{12}^{s,s} = T_{23}^{s,s} = T_{34}^{s,s} = T_{41}^{s,s}$, $T_{14}^{s,s} = T_{43}^{s,s} = T_{32}^{s,s} = T_{21}^{s,s}$ and $T_{13}^{s,s} = T_{31}^{s,s}$. The antisymmetric behaviour due to the inversion of B_{eff} according the spin polarization gives $T_{12}^{\uparrow\uparrow} = T_{14}^{\downarrow\downarrow}$ and $T_{14}^{\uparrow\uparrow} = T_{12}^{\downarrow\downarrow}$. Hence, it follows that

$$G_{\text{sH}}^{z} = \frac{e}{4\pi} 2 \left(T_{12}^{\uparrow\uparrow} - T_{14}^{\uparrow\uparrow} \right), \tag{17}$$

while the corresponding longitudinal charge conductance turns out to read

$$G_L = \frac{e^2}{h} \left(T_{13}^{\uparrow\uparrow} + \frac{T_{12}^{\uparrow\uparrow} + T_{14}^{\uparrow\uparrow}}{2} \right). \tag{18}$$

It is now clear that the non-vanishing G_{sH} stems from the symmetry breaking between probes 2 and 4 due to the effective magnetic field.

3.3. Computational approach

The calculation of the transmission amplitude is based on the simulation of classical trajectories of a large number of electrons with different initial conditions. We want to determine the probability $T_{1j}^{s,s'}$ of an electron with spin s to be transmitted to lead j when it is injected in lead 1. This coefficient can be determined from classical dynamics of electrons injected at $y_0 = -7.5 l_\omega$ (emitter position) with an injection probability following a spatial distribution $p_0(x_0, y_0) \propto \mathrm{e}^{-x_0^2/l_\omega^2}$ as in [26]. The total energy ε of a single electron (in probe 1) is composed by the free electron energy ε_y^0 for motion along y and the energy of the transverse mode considered ε_x^0 due to the parabolic confinement ($\varepsilon_x = \hbar\omega_d/2$ for the lowest channel).

Thus, we have calculated T_{ij}^{s} determined by numerical simulations of the classical trajectories injected into the junction potential V_c with boundary conditions [15] $\mathbf{r}(0) \equiv (x_0, y_0)$; $\mathbf{v}(0) \equiv \mathbf{v}_0$, each one with a weight $p_0(x_0)$. In general, these transmission amplitudes can depend on the position of the collectors along the probes.

Before the discussion about our results concerning the SHE we want to point out that a comparison with theoretical and experimental results allows us to test our approach. In fact, above we discussed the effects on the X-junction transport due to a quite small external magnetic field, B_{ext}, by focusing on the so-called *quenched region*. The measured 'quenching of the Hall effect' [21] is a suppression of the Hall resistance or 'a negative Hall resistance' R_{H} for small values of B_{ext}. The results reported in figure 2 (top), obtained by using our approach, show a good agreement with the experimental data figure 2 (bottom) by confirming the reliability of our approach, as can be understood by comparing top and bottom panels of figure 2. This behaviour can be explained in terms of the broken symmetry of the trajectories reported in figure 3. In the case of the SHE, the effective magnetic field is of a small intensity and not homogeneous. It is constant in the leads that constitute the junction and position dependent in the central zone of junction. It depends also on the spin and is directed upward or downward, according to the spin polarization along the z direction. It is very important to observe that all these properties, together with the low intensity of the effective field, characterize a transport regime which, in analogy with the known regime of the Hall effect, is called the quenching regime of the SHE [15].

4. Results

Applying the Büttiker–Landauer formula to the cross junction after the calculation of the transmission coefficients, we are able to compute some measurable quantities. The key issue

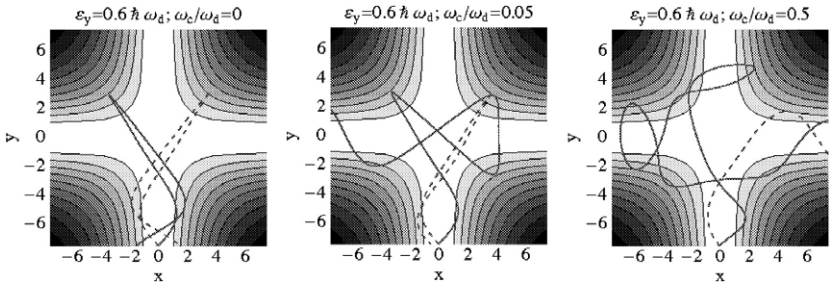

Figure 3. Simulated trajectories of electrons inside the junction for a Fermi energy ε_F corresponding to $\varepsilon_y = 0, 6\hbar_{\omega_d}$ and different values of the magnetic field. For every box there are two trajectories corresponding to different boundary conditions: positive $v_x(0)$ (continuous lines) and negative $v_x(0)$ (dashed lines). All trajectories start from the bottom (1) probe. For a vanishing magnetic field the trajectories are perfectly symmetric, but when the field grows the symmetry is broken. At weak fields ($\omega_c \sim 0.05\omega_d$) just one electron is found in probe 2 and quenching occurs. When the field grows further ($\omega_c \sim 0.5\omega_d$), both electrons are found in probe 4; thus, we are in the normal QHE regime. Looking at figure 2 we can understand the way the quenching and the normal QHE are realized at the microscopic level: i.e. by a symmetry-breaking mechanism that is macroscopically measured as a negative resistance.

for spintronics applications is to detect (at least indirectly [27]) a pure spin Hall current flowing out of multiterminal structures.

In figure 4 we show the spin Hall conductance $G^z_{\mathrm{sH}} = G^s_{24}$ (corresponding to the detection of the z component of the pure spin current I^s_2) for the crossing nanojunction as a function of the Fermi energy ε_F (right panels). The left panels also show the longitudinal charge conductance G_L of our four-terminal device depicted in figure 1. We have chosen significantly different values of the effective magnetic field (ω_c between 10^{-4} and $10^{-1}\omega_d$). The plots are obtained by our computational model, varying the Fermi energy and calculating the trajectories inside the junction.

When the effective magnetic field is large ($\omega_c \sim 10^{-1}\omega_d$, top panels of figure 4) by a comparison we point out the correspondence between the peaks in the charge conductance and those in the spin conductance. This could be very important from the experimental point of view since it should be not so difficult to recognize a peak in the longitudinal charge conductance. When we are in these circumstances we are sure to be in a condition to have a maximum of the spin conductance.

When the ratio ω_c/ω_d decreases (bottom panels of figure 4) we are in the typical regime of quenching, and several oscillations are predicted in the spin Hall conductance. It is not possible in this case to carry out a correspondence with the behaviour of the longitudinal charge conductance.

In the above, we discussed the observed Hall conductance (figure 2) and explained it in terms of the broken symmetry of the trajectories due to the presence of an external magnetic field (figure 3). The charge and spin conductance in figure 4 can be explained on the same grounds. Here the symmetry of the trajectories of spin up/spin down electrons is broken, as we show in figure 5.

Now we introduce a dimensionless quantity P_z to describe the polarization along the S_z spin axis of the current transmitted through the transverse probes of the junction, which is defined by

$$P_z = \frac{I_2^{\uparrow} - I_2^{\downarrow}}{I_2^{\uparrow} + I_2^{\downarrow}} = \frac{T_{12}^{\uparrow\uparrow} - T_{12}^{\downarrow\downarrow}}{T_{12}^{\uparrow\uparrow} + T_{12}^{\downarrow\downarrow}}.$$

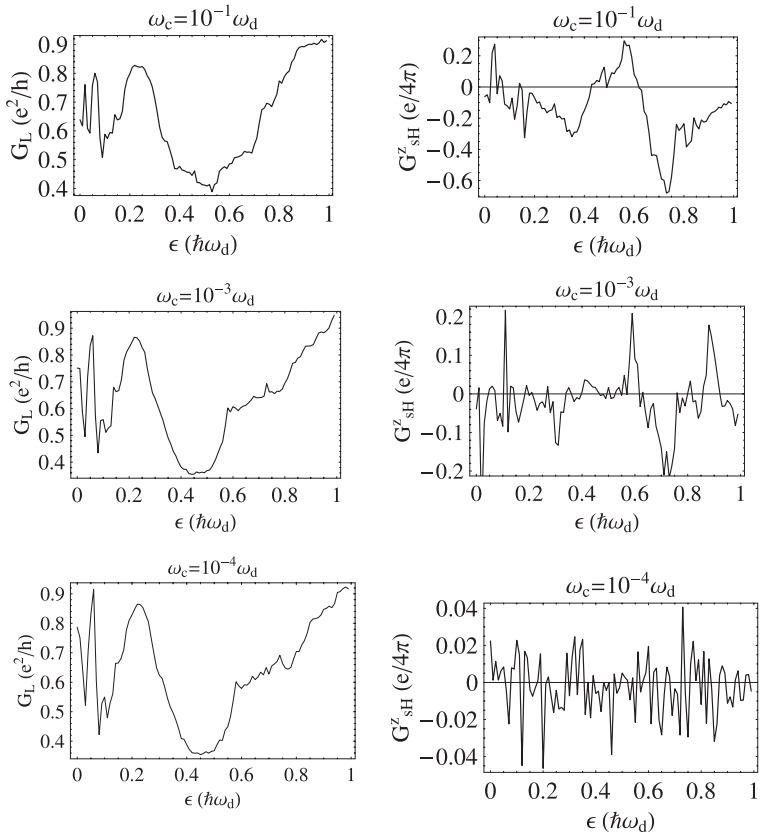

Figure 4. These diagrams show the spin and the charge conductance as a function of the Fermi energy. Top: for strong effective fields ($\omega_c \sim 10^{-1}\omega_d$) we underline that, when there are peaks for the charge conductance, we observe peaks for the spin conductance in the orthogonal direction. This circumstance is useful for the experimental measurability of the spin Hall current. Bottom: for weak effective fields ($\omega_c \lesssim 10^{-3}\omega_d$) it is not possible to establish a correspondence of G_{sH} with the behaviour of the G_L and several oscillations are predicted. However, note that oscillations are not much suppressed by the reduction of the effective field.

Here P_z is similar to the spin injection rate defined in ferromagnetic/semiconductor/ferromagnetic heterostructures [28], and it can be measured experimentally. The values of P_z are plotted in figure 6 as a function of the Fermi energy for two different strengths of the effective field. Note that a significant spin polarization in the transverse current is present also for weak effective magnetic fields.

In order to make the presence of a spin current observable, it can be useful to analyse the spin accumulation, i.e., the transverse profile of the out-of-plane $\langle S_z(\mathbf{r})\rangle$ component of the spin. As discussed in [20] the spin accumulation develops two peaks of opposite signs at the lateral edges of a 2DEG and, upon reversing the bias voltage, the edge peaks flip their sign. The behaviour outlined here, for the phase-coherent transport regime at low temperatures, is similar to the general phenomenology of the SHE which has been demonstrated convincingly, in some recent experiments [29], which focus on the optical detection of the spin Hall accumulation of opposite signs on the lateral edges of two-probe semiconductor structures.

The one-dimensional spatial transverse profile of $\langle S_z(\mathbf{r})\rangle$ across the lateral probes of the junction is plotted in figure 7 for the ballistic regime in the presence of β-SOC. The value

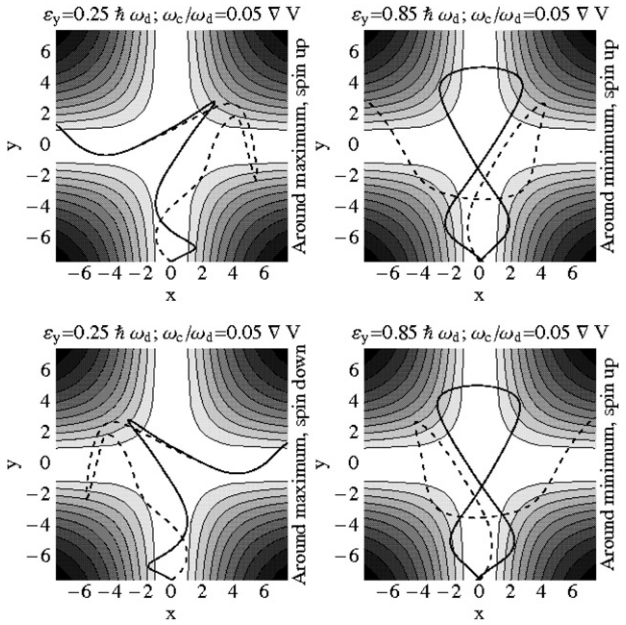

Figure 5. Simulated trajectories of electrons inside the junction with ε_F around the maximum and respectively the minimum of the calculated values for spin accumulation. The strength of SOC depends on the position in the junction. There are two trajectories plotted for a positive velocity $v_x(0)$. The trajectories start from the bottom. It is interesting to note that the symmetry of the trajectories is broken when we are near the peaks of spin accumulation.

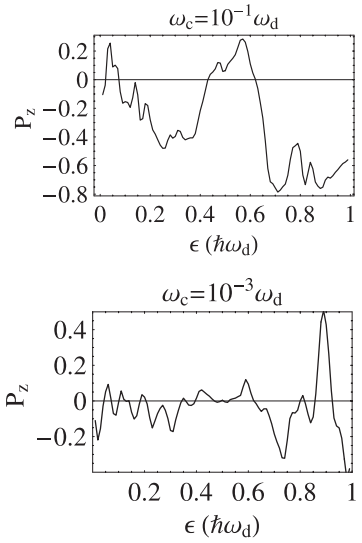

Figure 6. The spin polarization of the transverse current as a function of the Fermi energy, for two values of the effective field: (top) $\omega_c = 10^{-1}\omega_d$, (bottom) $\omega_c = 10^{-3}\omega_d$.

of $\langle S_z(\mathbf{x})\rangle$ which we found in the transverse probes (2, 4) is of order $10^{-1} - 10^{-2}\hbar/2$ for significative values of the effective magnetic field, as we show in figure 7.

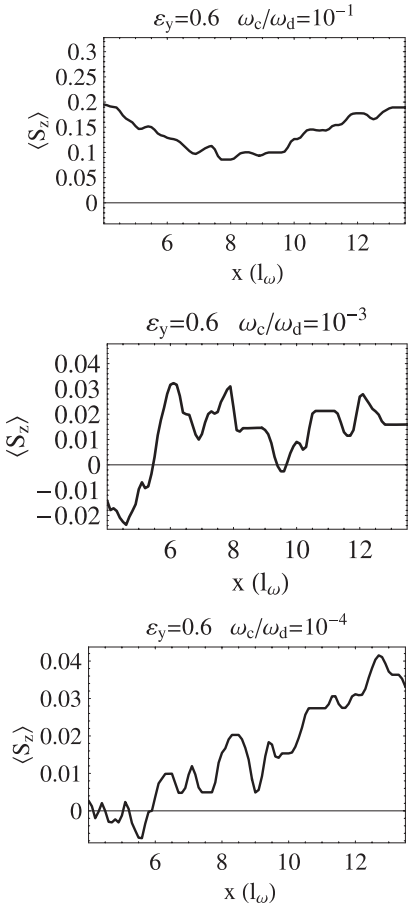

Figure 7. We have plotted the values of the one-dimensional transverse spatial profile of the spin accumulation $\langle S_z(x)\rangle$ in units of $\hbar/2$ across the transverse probes (2 and 4) for three values of the effective field: $\omega_c = 10^{-1}\omega_d$, $\omega_c = 10^{-3}\omega_d$, $\omega_c = 10^{-4}\omega_d$. It is possible to deduce the presence of quenching of the spin Hall effect by negative spin accumulation. The x coordinate indicates the position of the detector along the probe of the junction. We only used values from 2 l_ω to 14 l_ω.

As it turns out that $\langle S_z(x,0)\rangle = \langle S_z(-x,0)\rangle$, the transverse profile of the out-of-plane $S_z(\mathbf{r})$ component of the spin accumulation in the X-shaped junction develops two peaks of opposite signs in the lateral probes of the junction (2 and 4 in figure 1) when an unpolarized spin current is injected in the lead 1. Upon reversing the bias voltage (V_{13}), the edge peaks flip their sign $\langle S_z(\mathbf{r})\rangle_V = -\langle S_z(\mathbf{r})\rangle_{-V}$.

When transverse leads (2 and 4) are attached to the lateral edges of the 2DEG as in [20], the nonequilibrium spin accumulation pushes the pure spin current

$$I_{\mathrm{sH}} = \frac{\hbar}{2e}(I_2^{\uparrow} - I_2^{\downarrow})$$

into the transverse probes.

5. Conclusions

The four-probe junction discussed in this paper appears to be like a kind of ultra-sensitive scale, capable of reacting to the smallest variations of the magnetic field. In this case, any breakdown

of the symmetry (due to an external magnetic field) produces a Hall current. The effect should be observable even for what concerns the SO effect, especially for the so-called β coupling. In this case we found that a non-vanishing spin Hall conductance can be measured. As we showed in figure 4, the peaks in the pure spin Hall current, $I_{\rm SH}$, are present near the measurable peaks in the longitudinal charge conductance for $\omega_c \sim 10^{-1}\omega_d$, while the correlation between G_L and $G_{\rm sH}$ disappears in the quenching regime. All of our calculations are limited to the lowest subband but can be easily extended to the several-subband case.

This spin accumulation, corresponding to a transverse pure spin current flowing in the junction, can be a fundamental, observable signature of the spin Hall effect in four-probe devices such as the one analysed here. The value of the spin accumulation predicted in this paper for the β-SOC is some orders of magnitude larger than that predicted in [20] and due to a quite strong α-SOC. There it was found that $\langle S_z(x)\rangle \lesssim 10^{-3}$, i.e. two orders of magnitude smaller than the values found by us. Thus we can conclude that in narrow ballistic junctions the β-SOC could be quite relevant in order to obtain an efficient spin filtering.

The experimental feasibility of the nanojunction presented above obviously depends on its size and the materials. The fundamental parameter in our discussion is given by the ratio ω_c/ω_d, corresponding to λ^2/l_ω^2, i.e., the ratio between a material-dependent parameter λ and a size-dependent one l_ω (that can be assumed to be a fraction of the real width, W, of the probes).

The SO strengths have been evaluated for some semiconductor compounds such as QWs ($W \sim 100$) patterned in InGaAs/InP heterostructures, where λ^2 takes values between 0.5 and 1.5 nm^2 ($\hbar\omega_{\rm c} \sim 10^{-6}$–$10^{-4}$ eV $\leftrightarrow$ $\omega_{\rm c}/\omega_d \sim 10^{-4}$–$10^{-3}$). For GaAs heterostructures, λ^2 is one order of magnitude smaller (~ 4.4 Å^2) than in InGaAs/InP, whereas for HgTe-based heterostructures it can be more than three times larger [30].

Since the lithographical width of a wire defined in a 2DEG can be as small as 20 nm [31] we can realistically assume that $\omega_{\rm c}/\omega_d$ runs from 1×10^{-6} to 1×10^{-1}.

Acknowledgment

We acknowledge the support of the grant 2006 PRIN 'Sistemi Quantistici Macroscopici-Aspetti Fondamentali ed Applicazioni di strutture Josephson Non Convenzionali'.

References

[1] Awschalom D D, Loss D and Samarth N 2002 *Semiconductor Spintronics and Quantum Computation* (Berlin: Springer)
Kane B E 1998 *Nature* **393** 133
[2] Wolf S A, Awschalom D D, Buhrman R A, Daughton J M, von Molnar S, Roukes M L, Chtchelkanova A Y and Treger D M 2001 *Science* **294** 1488
[3] Chien C L and Westgate C W (ed) 1980 *The Hall Effect and its Applications* (New York: Plenum)
[4] D'yakonov M I and Perel' V I 1971 *JETP Lett.* **13** 467
[5] Murakami S, Nagaosa N and Zhang S C 2003 *Science* **301** 1348
[6] Sinova J, Culcer D, Niu Q, Sinitsyn N A, Jungwirth T and MacDonald A H 2004 *Phys. Rev. Lett.* **92** 126603
[7] Sheng M L, Sheng D N and Ting C S 2005 *Phys. Rev. Lett.* **94** 016602
Hankiewicz E M, Molenkamp L W, Jungwirth T and Sinova J 2004 *Phys. Rev.* B **70** 241301(R)
[8] Moroz A V and Barnes C H W 2000 *Phys. Rev.* B **61** R2464
[9] Kelly M J 1995 *Low-Dimensional Semiconductors: Material, Physics, Technology, Devices* (Oxford: Oxford University Press)
[10] Thornton T J, Pepper M, Ahmed H, Andrews D and Davies G J 1986 *Phys. Rev. Lett.* **56** 1198
[11] Bellucci S and Onorato P 2003 *Phys. Rev.* B **68** 245322
[12] Bellucci S and Onorato P 2005 *Phys. Rev.* B **72** 045345
[13] Bellucci S and Onorato P 2006 *Phys. Rev.* B **73** 045329

[14] Bernevig B A and Zhang S C 2006 *Phys. Rev. Lett.* **96** 106802
[15] Bellucci S and Onorato P 2006 *Phys. Rev.* B **74** 245314
[16] Hattori K and Okamoto H 2006 *Phys. Rev.* B **74** 155321
[17] Jiang Y and Hu L 2006 *Preprint* cond-mat/0603755
[18] Büttiker M 1986 *Phys. Rev. Lett.* **57** 1761
[19] Nikolic B K, Zarbo L P and Souma S 2005 *Phys. Rev.* B **72** 075361
[20] Nikolic B K, Souma S, Zarbo L P and Sinova J 2005 *Phys. Rev. Lett.* **95** 046601
[21] Ford C J B, Washburn S, Büttiker M, Knoedler C M and Hong J M 1989 *Phys. Rev. Lett.* **62** 2724
[22] Thornton T J 1995 *Rep. Prog. Phys.* **58** 311
[23] Laux S E, Frank D J and Stern F 1988 *Surf. Sci.* **196** 101
Drexler H *et al* 1994 *Phys. Rev.* B **49** 14074
Kardynal B *et al* 1997 *Phys. Rev.* B **55** R1966
[24] Pareek T P 2004 *Phys. Rev. Lett.* **92** 076601
[25] Kiselev A A and Kim K W 2003 *J. Appl. Phys.* **94** 4001
[26] Geisel T, Ketzmerick R and Schedletzky O 1992 *Phys. Rev. Lett.* **69** 1680
[27] Dyakonov M I and Perel V I 1971 *JETP Lett.* **13** 467
Hirsch J E 1999 *Phys. Rev. Lett.* **83** 1834
Hankiewicz E M *et al* 2004 *Phys. Rev.* B **70** 241301(R)
[28] Johnson M 1998 *Phys. Rev.* B **58** 9635
Johnson M and Silsbee R H 1988 *Phys. Rev.* B **37** 5326
[29] Kato Y K *et al* 2004 *Science* **306** 1910
Wunderlich J *et al* 2005 *Phys. Rev. Lett.* **94** 047204
[30] Zhang X C, Pfeuffer-Jeschke A, Ortner K, Hock V, Buhmann H, Becker C R and Landwehr G 2001 *Phys. Rev.* B **63** 245305
[31] Knop M, Richter M, Maßmann R, Wieser U, Kunze U, Reuter D, Riedesel C and Wieck A D 2005 *Semicond. Sci. Technol.* **20** 814